Direct Torque Control of Synchronous Reluctance Motor using Feedback Linearization Including Saturation and Iron Losses

H. Abootorabi Zarchi, Faculty of Electrical & Computer Engineering, Isfahan University of Technology, Isfahan, Iran
Gh. R. Arab Markadeh, Department of Engineering, Shahrekord University, Shahrekord, Iran
J. Soltani, Faculty of Electrical & Computer Engineering, Isfahan University of Technology, Isfahan, Iran

Keywords: Synchronous Reluctance Motor, Input-Output Feedback Linearization, Magnetic Saturation and Iron Losses, Stator Resistance Estimator, Lagrange's Theorem

Summary

In this paper, a nonlinear controller capable of high dynamic torque regulation is introduced for Synchronous Reluctance Motor (SynRM) drive on the basis of input-output feedback linearization considering the different strategies related to this motor. The control strategies considered are: maximum torque per Ampere (MTPA), minimum KVA rating for the inverter and efficiency-optimized control. The proposed nonlinear controller is capable of regulating the motor torque by selecting the product of d and q axes torque currents as one of the output variables. As a result, the nonlinear and cross-coupling aspects between the d and q axes torque currents and the terminal currents can be eliminated. Hence, the linear torque-speed characteristics can be achieved. In addition, absolute implementation of strategies needs motor parameters with sufficient accuracy. The stator direct axis inductance (Ld) and iron loss resistance (Ri) are regarded and a PI estimator is presented to estimate the stator resistance variation. Finally, simulation and practical results are included throughout the paper to illustrate and verify the theoretical considerations.

Introduction

In recent years, the synchronous reluctance motor (SynRM) received much attention for many applications due to its simple and rugged construction [1-3]. A SynRM is advantaged on induction motor by the absence of rotor copper losses, on brushless motors by inexpensive rotor structure, and on switched reluctance motor by a much lower torque ripple and low noise. Compared to surface type permanent magnet synchronous motor (SPMSM), it is capable of high-speed operation and for use in high-temperature environments. The earlier designs of SynRMs have limited saliency ratio, which results in low power factor and low torque density. However, these drawbacks have been overcome by introducing axially laminated rotor designs. Moreover, in an inverter-fed SynRM, cage windings are not required for starting purpose. Accordingly, it becomes possible to design rotors of higher saliency ratio. From control point of view, a SynRM has some advantages such that it can be considered an alternative to induction motor in many applications, such as in robotics, traction and low-cost drives. Also the SynRM is suitable for super high-speed applications in machine tools and molecular pumps [4].

For high performance SynRM drive, it is desirable to achieve optimum operation at maximum torque per Ampere (MTPA), high efficiency and maximum power factor [4, 5]. Detailed discussions and analysis of the control of a SynRM is given in reference [6]. The analysis is restricted to the ideal motor, in which saturation and iron losses are ignored. However, the control of the SynRM is highly affected by both magnetic saturation and presence of iron losses [7]. Accurate representation of saturation effects requires detailed knowledge of magnetic behavior in both d and q axes along with cross-saturation at different operating conditions. Due to the high reluctance associated with q-axis, it may be sufficient to consider magnetic saturation in d-axis only. The iron loss is considered in the SynRM by adding a shunt resistor in both d and q equivalent circuits. Some research efforts have been done to compensate for the saturation and iron losses in the vector controlled SynRM model. A compensated vector control scheme has been proposed in [8]. Two current observers are used to allow for the difference between the stator currents and the currents that govern the developed torque. Neglecting iron loss, the effect of magnetic saturation on control of the SynRM has been discussed [9]. It is assumed that d-axis and q-axis inductances saturate to the same level under all operating conditions. In [10], the motor parameters are online estimated on the basis of (RLS) method, only using the proposed mathematical method and motor measured currents and voltages. In [11], the iron losses resistance is obtained by no load test and the magnetic saturation is considered through a lookup table which shows the variation of direct axis inductance versus direct axis current while the little effect of magnetic saturation on parameter L_q is ignored.

Although many papers discuss the direct torque control (DTC) of induction motors [12-14], only a few papers study the DTC for SynRMs. For example, Consoli et al. [15] proposed a sensorless torque control for SynRM Drives. In this paper, however only PI controllers were used. As a result, the transient responses and load disturbance responses were not satisfactory. To solve the problem, in [16] an adaptive backstepping controller and a model reference adaptive controller were proposed for a SynRM direct torque control system. By using the proposed controllers, the transient responses and load disturbance rejection capability are obviously improved. However, in these conventional DTC schemes, the SynRM torque is indirectly regulated through the d and q axis terminal currents control, as in other types of a.c. motor drives, and thus, the high performance of the internal current loop is indispensable. Several difficulties in high dynamic current control can be encountered due to the limitation of inverter voltage and its switching frequency, the cross-coupling effects between d and q axis currents, the saturation of each current controller, and so on. If the iron losses of the SynRM are considered, these effects become more severe. The nonlinearity and coupling effects between the terminal currents and torque currents result in the deterioration of the torque dynamic performance and linearity of torque control. To overcome the above drawbacks, in [17] a nonlinear method capable of high dynamic torque control of SynRM

has been described based on input-output feedback linearization (IOFL) DTC space vector modulation (DTC-SVM). In the presented scheme, the efficiency optimization criterion and the motor torque are chosen as output variables and two-axis inductances and stator resistance (R_s) are assumed constant. Since the torque can be regulated directly by selecting the product of d and q axes torque currents as one of the output variables, the nonlinear and cross-coupling aspects between the d and q axes torque currents and the terminal currents due to the iron losses can be eliminated. Hence, the linear torque-speed characteristic can be achieved.

In general, the variation of stator resistance due to changes in temperature or frequency deteriorates the drive performance by introducing errors in the estimated d and q axis stator fluxes. IOFL technique also, requires the full knowledge of the motor parameters with sufficient accuracy. Several control schemes have been proposed to overcome this issue [18, 19]. These methods suffer from shortcomings such as restriction of the control range, problem of convergence and a lack of speed of response. A novel study [20] proposed the use of stator current error with a proportional plus integral (PI) estimator, presenting a good performance for tuning the stator resistance of an induction motor drive. The main concept of this method of stator resistance compensation using stator current phasor error has been applied in permanent magnet synchronous motor drives [21]. In [21], the error between actual and reference currents is processed through a PI controller. This, in fact, determines the change in the controller effort when stator resistance changes for some reason.

The main purpose of this paper is to introduce a nonlinear controller for SynRM drive on the basis of IOFL by continuing the research work described in [17] for the following gains:

– to implement of MTPA and minimum input motor KVA rating control strategies, besides of efficiency-optimized scheme experimented in [17];
– to include saturation effects and stator resistance variations besides of iron loss considered in [17].

The stator resistance is predicted by a PI estimator in this paper. This estimator observes the error between reference and actual fluxes and online determines the stator resistance variations corresponding to this error. To confirm the validity of the presented approach, simulation and experiments are carried out.

SynRM model including iron losses

In the synchronously rotating reference frame, the d and q axes equivalent circuits for the SynRM, including iron losses, are shown in Fig.1 [11]. Note that the resistance R_i represents the iron losses connected in parallel to both rotational and transient back EMF in this figure. From the equivalent circuit, we obtain that the electromagnetic torque T_e is proportional to the vector product of flux linkages and currents and can be obtained as (1), where P denotes the number of poles, L_d and L_q represent d and q axes inductances, respectively. Since R_i supplies an additional current path to each axis equivalent circuit, the torque does not depend on measured terminal current, i^e_{ds} and i^e_{qs}, but on i^e_{dT} and i^e_{qT}. Hence, the terminal currents can no longer directly govern the torque.

$$T_e = \frac{3}{2}\frac{P}{2}.(\lambda^e_{ds}.i^e_{qT} - \lambda^e_{qs}.i^e_{dT}) = \frac{3}{2}\frac{P}{2}.(L_d - L_q).i^e_{dT}.i^e_{qT} = K_T i^e_{dT}\, i^e_{qT} \tag{1}$$

$$\text{Where } K_T = \frac{3}{2}\frac{P}{2}\cdot\left(L_d - L_q\right)$$

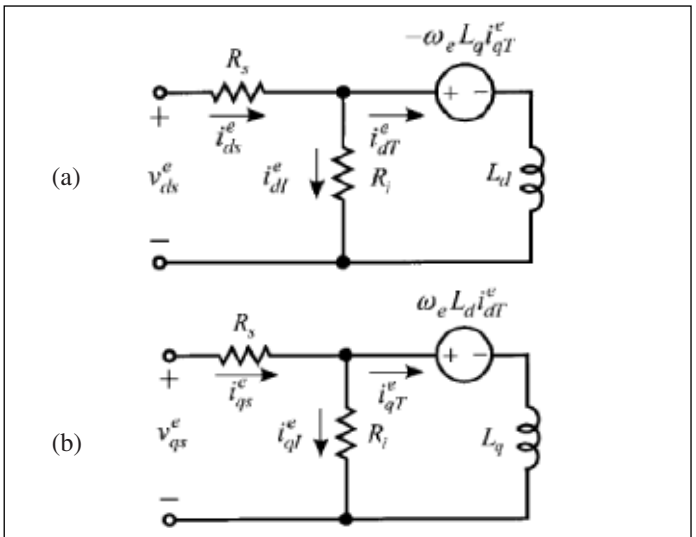

Fig. 1: Equivalent circuits for SynRM considering the iron losses. (a) d-axis. (b) q-axis.

From Fig. 1, the currents that are responsible for torque production, i^e_{dT} and i^e_{qT}, can be described as (2) with respect to the terminal currents i^e_{ds} and i^e_{qs}

$$\begin{bmatrix} i^e_{dT} \\ i^e_{qT} \end{bmatrix} = \frac{R_i}{(d/dt + R_i/L_d)(d/dt + R_i/L_q) + \omega_e^2} \begin{bmatrix} (d/dt + R_i/L_q)/L_d & \omega_e/L_d \\ -\omega_e/L_q & (d/dt + R_i/L_q)/L_q \end{bmatrix} \begin{bmatrix} i^e_{ds} \\ i^e_{qs} \end{bmatrix} \tag{2}$$

As shown in (2), very large value of R_i makes i^e_{dT} and i^e_{qT} identical to i^e_{ds} and i^e_{qs}, regardless of rotational speed ω_e. Therefore, the vector control of the SynRM with decoupled d and q circuits can be easily performed and it can be easily determined that the optimal angle for maximum torque per Ampere is equal to 45° [6]. However, considering actual value of R_i produces the cross-coupling effects between the d and q circuits in (2), resulting in an additional angle shift between the torque current and terminal current vector as shown in Fig. 2 [7]. This misalignment brings out the steady-state torque error and makes the optimal angle of each strategy different from that of the infinite R_i case. Consequently, for high dynamic torque regulation and every strategy of the SynRM when the iron losses are included, the compensation of the cross-coupling term is required and the voltage equations for the SynRM should be expressed using the torque currents, rather than the terminal currents, as

$$v^e_{ds} = R_s i^e_{dT} + L_d \frac{di^e_{dT}}{dt} - (1 + \frac{R_s}{R_i})\omega_e L_q i^e_{qT} \tag{3}$$

$$v^e_{qs} = R_s i^e_{qT} + L_q \frac{di^e_{qT}}{dt} + (1 + \frac{R_s}{R_i})\omega_e L_d i^e_{dT} \tag{4}$$

Choosing $i^e_{dT} = x_1$, $i^e_{qT} = x_2$, $\omega_e = x_3$ as states and $v^e_{ds} = u_1$, $v^e_{qs} = u_2$ as inputs, the nonlinear dynamic model for the SynRM considering iron losses can be described in the following standard state-variable form:

$$\dot{X} = f(X) + g(X)U \tag{5}$$

where

$$X=\begin{bmatrix} x_1 & x_2 & x_3 \end{bmatrix}^{\mathrm{T}},\quad U=\begin{bmatrix} u_1 & u_2 \end{bmatrix}^{\mathrm{T}}$$

$$f(X)=\begin{bmatrix} f_1 \\ f_2 \\ f_3 \end{bmatrix}=\begin{bmatrix} -\frac{R_s}{L_d}x_1+\frac{L_q}{L_d}(1+\frac{R_s}{R_i})x_2x_3 \\ -\frac{R_s}{L_q}x_2-\frac{L_d}{L_q}(1+\frac{R_s}{R_i})x_1x_3 \\ (\frac{3P(L_d-L_q)}{4J_m}x_1x_2-\frac{T_l}{J_m})/\frac{P}{2}-\frac{B_m x_3}{J_m} \end{bmatrix}, \tag{6}$$

$$g(X)=\begin{bmatrix} g_1 & g_2 \end{bmatrix}=\begin{bmatrix} \frac{1}{L_d} & 0 \\ 0 & \frac{1}{L_q} \\ 0 & 0 \end{bmatrix}$$

where J_m is he rotor moment of inertia and B_m is the friction coefficient.

Note that the interactions between the d and q axes torque currents and SynRM angular speed are modeled, and the whole system is nonlinear and coupled.

Control objectives of SynRM strategies

In this paper, the three well-known strategies of SynRM (MTPA, efficiency-optimized and minimum input KVA) are investigated under the constraint of constant torque production. In MTPA strategy, the minimization of SynRM stator current, in efficiency-optimized scheme, the minimization of input active power and in minimum input KVA, the minimization of SynRM input apparent power is selected as control objective. Based on Lagrange's Theorem, it can be easily found that each strategy is satisfied when the torque curve and control objective curve are tangent at a point.

MTPA control

The maximum torque per Ampere can be obtained by minimizing the expression for the stator current under the condition of constant torque production at a certain speed.

The square of the stator current I_s^2 of the SynRM can be calculated as

$$I_s^2=i_{ds}^{e^2}+i_{qs}^{e^2}=\left(i_{dT}^e+i_{dI}^e\right)^2+\left(i_{qT}^e+i_{qI}^e\right)^2 \tag{7}$$

where i_{dl}^e and i_{ql}^e are the currents responsible for iron losses, which can be calculated as

$$i_{dI}^e=-\omega_e\frac{L_q}{R_i}i_{qT}^e$$
$$i_{qI}^e=\omega_e\frac{L_d}{R_i}i_{dT}^e \tag{8}$$

Thus, the stator current vector can be expressed as (9) using (7-8)

$$I_s^2=i_{dT}^{e^2}+i_{qT}^{e^2}+\frac{1}{R_i^2}(L_d^2i_{dT}^{e^2}+L_q^2i_{qT}^{e^2})\omega_e^2+\frac{2}{R_i}(L_d-L_q)i_{dT}^ei_{qT}^e\omega_e \tag{9}$$

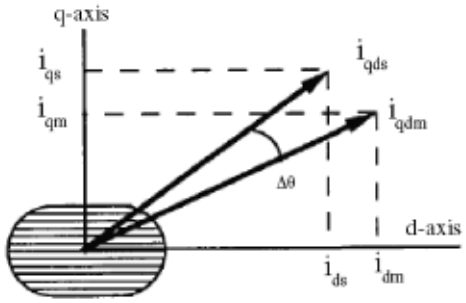

Fig. 2 : The angle displacement between torque current (i_{dqT}^e) and terminal current (i_{dqs}^e) vectors

Efficiency-optimized control

The maximum efficiency method can be obtained by minimizing the expression for the power into the machine under the constraint of constant power output.

The input power P_{in} of the SynRM is obtained as

$$P_{in}=\frac{3}{2}(V_{ds}^eI_{ds}^e+V_{qs}^eI_{qs}^e) \tag{10}$$

Using (3-8) in steady-state condition, P_{in} can be expressed as (11)

$$P_{in}=R_s(i_{dT}^{e\,2}+i_{qT}^{e\,2})+\frac{1}{R_i}(1+\frac{R_s}{R_i})(L_d^2i_{dT}^{e^2}+L_q^2i_{qT}^{e^2})\omega_e^2 +\frac{2R_s}{R_i}(L_d-L_q)i_{dT}^ei_{qT}^e\omega_e \tag{11}$$

Minimum Input KVA

In order to obtain an expression for the minimum input KVA, one can minimize input apparent power S_{in} under the condition of constant power output.

The input apparent power S_{in} of the SynRM is obtained as

$$S_{in}^2=V_s^2I_s^2=\left(v_d^2+v_q^2\right)I_s^2 \tag{12}$$

Using (2-12) in steady-state condition and ignoring R_s for simplification in following equations, S_{in} can be expressed as

$$S_{in}^2=\frac{\omega_e^4}{R_i^2}\left(L_d^4i_d^{T4}+L_q^4i_q^{T4}\right)+\omega_e^2\left(L_d^2i_d^{T4}+L_q^2i_q^{T4}\right) +\frac{2\omega_e^3}{R_i}\left(L_d-L_q\right)\left(L_d^2i_d^{T3}i_q^T+L_q^2i_d^Ti_q^{T3}\right) \tag{13}$$

In this paper, the minimization of equation (9), (11) or (13) is regarded as one of the control objectives under the constraint of constant torque production. In Fig. 3, according to equation (1), the constant torque curve can be drawn as a hyperbola on the $x_1 - x_2$ plane. On the same plane, at a speed, a curve representing every strategy, takes the form of an ellipse. Under the constraint of constant torque production, if an operating point is set at point "a" in Fig. 3, the curve A is supposed to be a control objective curve (for example, constant stator current curve). If an operating point is set at "b", the curve B is another control objective curve. Based on Lagrange's Theorem, it can be easily found that control objective is minimum when the torque curve and control objective

curve are tangent at a point if and only if their gradient vectors are parallel. This means that $\nabla T_e(x_1, x_2)$ must be a scalar multiple of $\nabla(I_s^2, P_{in}$ or $S_{in}^2)$ at the point of tangency (see "b" in Fig. 3), so that

$$\left\|\nabla T_e(x_1,x_2)\right\|\left\|\nabla I_s^2(x_1,x_2)\right\|\sin\theta = 0$$

in MTPA (14)

$$\left\|\nabla T_e(x_1,x_2)\right\|\left\|\nabla P_{in}(x_1,x_2)\right\|\sin\theta = 0$$

in Efficiency-Optimized Control (15)

$$\left\|\nabla T_e(x_1,x_2)\right\|\left\|\nabla S_{in}^2(x_1,x_2)\right\|\sin\theta = 0$$

in Minimum input KVA (16)

Where θ is the angle between $\nabla T_e(x_1, x_2)$ and $\nabla(I_s^2, P_{in}$ or $S_{in}^2)$.

Feedback linearization control of SynRM

By the state feedback linearization control, the nonlinear motor system transforms into a linear one by a nonlinear feedback, and then use the well-known linear design techniques to complete the control design [22].

Selection of outputs

To achieve the control objectives, choosing the torque and the magnitude of the cross product of $\nabla T_e(x_1, x_2)$ and $\nabla(I_s^2, P_{in}$ or $S_{in}^2)$ as output variables, output vector $[y_1 \quad y_2]^T$ can be defined as

$$y_1 = T_e = K_T x_1 x_2 \tag{17}$$

MTPA strategy

$$\begin{aligned} y_2 &= \left\|\nabla T_e(x_1,x_2)\right\|\left\|\nabla I_s^2(x_1,x_2)\right\|\sin\theta \\ &= 2K_T[(1+\frac{L_q^2}{R_i^2}x_3^2)x_2^2 - (1+\frac{L_d^2}{R_i^2}x_3^2)x_1^2] \end{aligned} \tag{18}$$

Efficiency-optimized control strategy

$$\begin{aligned} y_2 &= \left\|\nabla T_e(x_1,x_2)\right\|\left\|\nabla P_{in}(x_1,x_2)\right\|\sin\theta \\ &= 3K_T[(R_s+\frac{1}{R_i}(1+\frac{R_s}{R_i})L_d^2\omega_e^2)x_2^2 - (R_s+\frac{1}{R_i}(1+\frac{R_s}{R_i})L_q^2\omega_e^2)x_1^2 \end{aligned} \tag{19}$$

Min. input KVA strategy

$$\begin{aligned} &\left\|\nabla T_e(i_d^T,i_q^T)\right\|\left\|\nabla S_{in}^2(i_d^T,i_q^T)\right\|\sin\theta \\ &\Rightarrow \frac{x_3^2}{R_i^2}\left(L_q^4x_2^4 - L_d^4x_1^4\right) + \left(L_q^2x_2^4 - L_d^2x_1^4\right) \\ &+\frac{x_3}{R_i}\left(L_d - L_q\right)\left\{L_q^2x_2^3x_1^4 - L_d^2x_1^3x_2^4\right\} \end{aligned} \tag{20}$$

Obviously chosen control strategy would be carried out when y_2 can be maintained in zero value.

Taking the time derivatives of these outputs, respectively, until inputs u_i, $i = 1, 2$ appear in the derivative expressions of each output variable are as follows:

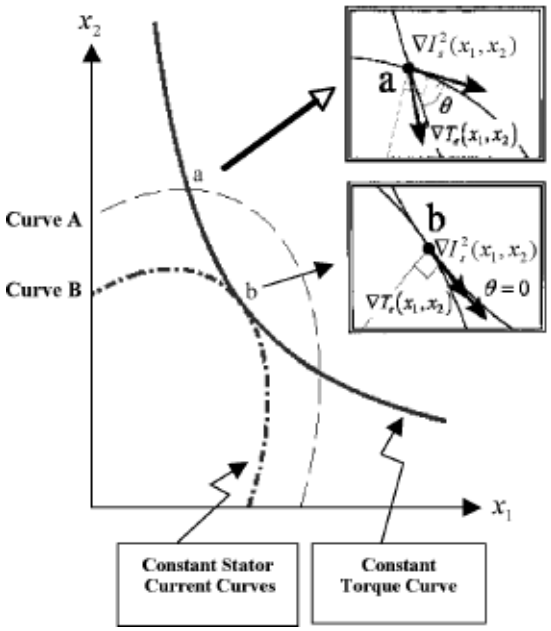

Fig. 3 : Constant torque curve and stator current curve on $x_1 - x_2$ plane

$$\begin{bmatrix}\dot{y}_1\\ \dot{y}_2\end{bmatrix} = \begin{bmatrix}L_f y_1\\ L_f y_2\end{bmatrix} + \begin{bmatrix}L_{g_1}y_1 & L_{g_2}y_1\\ L_{g_1}y_2 & L_{g_2}y_2\end{bmatrix}\begin{bmatrix}u_1\\ u_2\end{bmatrix} = \begin{bmatrix}L_f y_1\\ L_f y_2\end{bmatrix} + E(X)U \tag{21}$$

where $L_f y_i$, i = 1, 2 is the Lie derivative of y_i with respect to f. From (21), the relative degree of each output variable is equal to one ($r_1 = r_2 = 1$). The total relative degree of the SynRM model is $r = r_1 + r_2 = 2$ and is not equal to the number of state variables. Hence, there exist internal dynamics, which will be discussed later. $L_f y_i$ and $E(X)$ matrix can be derived straightforward and are described in the Appendix II. This decoupling matrix $E(X)$ is found to be nonsingular over all operating regions except null state by its determinant expressed in

$$\det(E(X)) = \frac{4K_T^2}{L_d L_q}[(x_1^2 + x_2^2) + \frac{1}{R_i^2}(L_d^2x_1^2 + L_q^2x_2^2)x_3^2] \quad \text{in MTPA} \tag{22}$$

$$\begin{aligned} \det(E(X)) = \frac{6K_T^2}{L_d L_q}&[R_s(x_1^2 + x_2^2) \\ &+ \frac{(R_s + R_i)}{R_i^2}(L_d^2x_1^2 + L_q^2x_2^2)x_3^2] \end{aligned} \quad \text{in Efficiency-optimized} \tag{23}$$

$$\det(E(X)) = \frac{2K_T}{L_d L_q}\left\{\begin{aligned}&\frac{2x_3^2}{R_i^4}\left(L_d^4x_1^4 + L_q^4x_2^4\right) + 2\left(L_d^2x_1^4 + L_q^2x_2^4\right)\\ &+\frac{1}{R_i}\left(L_d - L_q\right)\left(L_d^2x_1^2 + L_q^2x_2^2\right)x_1x_2x_3\end{aligned}\right\} \quad \text{in Min. input KVA} \tag{24}$$

The input–output feedback linearization and the decoupling control law can be selected as follows:

$$U = E^{-1}\begin{bmatrix}v_1 - L_f y_1\\ v_2 - L_f y_2\end{bmatrix} \tag{25}$$

By the input–output feedback linearization control, the original nonlinear and coupled SynRM system can be transformed to an exact linear and decoupled closed-loop system with each pole at the origin of the transformed state space as

$$\dot{y}_1 = v_1$$
$$\dot{y}_2 = v_2 \quad (26)$$

The overall block diagram of the proposed control algorithm is shown in Fig. 4. Given the torque reference T_e^*, the final d and q axes voltage references v_{ds}^{e*} and v_{qs}^{e*} are generated through the pseudo derivative feedback control and the linearization stages. The phase currents of the SynRM are transformed into d and q axes currents on the synchronously rotating reference frame using the position information of the SynRM. They are then converted into states for the proposed feedback linearization control.

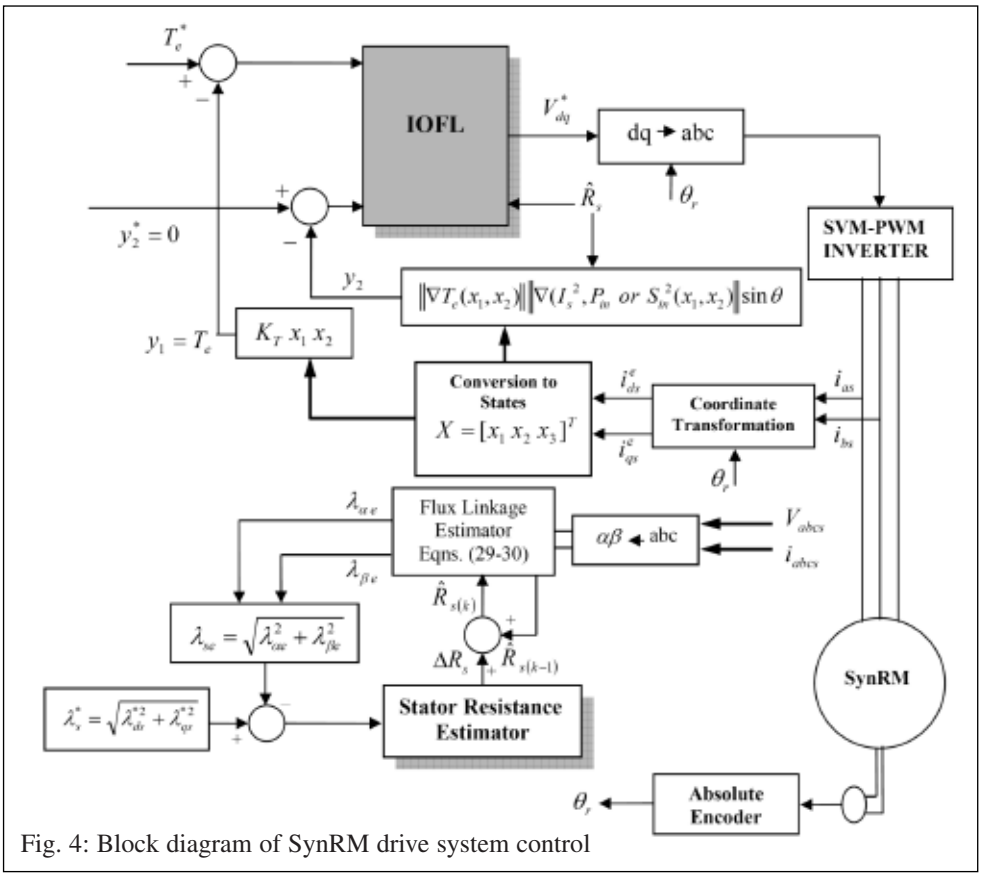

Fig. 4: Block diagram of SynRM drive system control

Internal dynamics

In this paper, the nonlinear dynamics of the SynRM can be decomposed into an input–output part as (26) and an unobservable one by input–output linearization technique because total relative degree is not equal to the number of states. Since the stability of the whole SynRM dynamics is influenced not only by the input–output part, but also by the unobservable part, the behavior of the internal dynamics must be investigated. The corresponding internal dynamics of the SynRM in this paper can be given as (27), and the zero dynamics for checking the stability of internal dynamics is given as (28), where all outputs are maintained at zero. Although the zero dynamics are marginally stable as (28), the actual dynamics are assumed to be asymptotically stable due to the mechanical losses and viscosity damping [22]. Therefore, the whole system is said to be asymptotically minimum phase, because the zero dynamics of the SynRM system is stable.

$$\dot{x}_3 = \left(\frac{3P}{4J_m}\left(L_d - L_q\right) i_{dT}^e i_{qT}^e - \frac{T_l}{J_m}\right) / \frac{P}{2} - \frac{B_m x_3}{J_m} \quad (27)$$

$$\dot{x}_3 = \left(-\frac{T_l}{J_m}\right) / \frac{P}{2} - \frac{B_m x_3}{J_m} \quad (28)$$

Stator resistance estimator of a SynRM drive system

The stator resistance changes due to the change in temperature during the operation of the machine as the machine losses change. The variation of the stator resistance is a thermal process and therefore is not only determined by the machine losses but also the time. The drive system may become unstable if the stator resistance value used in the controller differs from that of the machine resistance. Among the other variables of the machine, the stator flux vector is highly affected by the resistance changes particularly at low speed.

The stator flux linkage of SynRM is estimated by integrating the difference between the input voltage and the voltage drop across the stator resistance in stator reference frame as given by

$$\lambda_\alpha = \int_0^t \left(v_\alpha - R_s i_\alpha\right) dt + \lambda_\alpha\left(t = 0\right) \quad (29)$$

$$\lambda_\beta = \int_0^t \left(v_\beta - R_s i_\beta\right) dt + \lambda_\beta\left(t = 0\right) \quad (30)$$

$$\lambda_s = \sqrt{\lambda_\alpha^2 + \lambda_\beta^2} \quad (31)$$

Where v_α and v_β, i_α and i_β and and λ_α are $\alpha - \beta$ axis stator voltages, currents and flux linkages, respectively.

If there is no change in R_s, the actual stator flux (λ_{sa}) and estimated stator flux (λ_{se}) of the motor are given by

$$\lambda_s = \lambda_{sa} = \lambda_{se} = \int \left(v_s - R_s i_s\right) dt \quad (32)$$

Now, let the stator resistance of the motor change by ΔR_s, which causes a change in Δi_s in stator current vector, the corresponding changes in $\alpha - \beta$ axis currents are Δi_α and Δi_β, respectively. The controller uses the unchanged value of resistance while actual motor resistance changes. The actual stator flux (λ_{sa}) and estimated stator flux (λ_{se}) of the machine are given by (33-35),

$$\lambda_\alpha + \Delta\lambda_{\alpha a} = \int \left[v_\alpha - \left(i_\alpha + \Delta i_\alpha\right)\left(R_s + \Delta R_s\right)\right] dt \quad (33)$$

$$\lambda_\beta + \Delta\lambda_{\beta a} = \int \left[v_\beta - \left(i_\beta + \Delta i_\beta\right)\left(R_s + \Delta R_s\right)\right] dt \quad (34)$$

$$\lambda_s + \Delta\lambda_{sa} = \int \left[v_s - \left(i_s + \Delta i_s\right)\left(R_s + \Delta R_s\right)\right] dt \tag{35}$$

Estimated controller variables are

$$\lambda_\alpha + \Delta\lambda_{\alpha e} = \int \left[v_\alpha - \left(i_\alpha + \Delta i_\alpha\right) R_s \right] dt \tag{36}$$

$$\lambda_\beta + \Delta\lambda_{\beta e} = \int \left[v_\beta - \left(i_\beta + \Delta i_\beta\right) R_s \right] dt \tag{37}$$

$$\lambda_s + \Delta\lambda_{se} = \int \left[v_s - \left(i_s + \Delta i_s\right) R_s \right] dt \tag{38}$$

The errors in the estimated flux linkage from the actual flux linkage is given by

$$\Delta\lambda_\alpha = \Delta\lambda_{\alpha e} - \Delta\lambda_{\alpha a} = \int \left(i_\alpha + \Delta i_\alpha\right)\Delta R_s \, dt \tag{39}$$

$$\Delta\lambda_\beta = \Delta\lambda_{\beta e} - \Delta\lambda_{\beta a} = \int \left(i_\beta + \Delta i_\beta\right)\Delta R_s \, dt \tag{40}$$

$$\Delta\lambda_s = \Delta\lambda_{se} - \Delta\lambda_{sa} = \int \left(i_s + \Delta i_s\right)\Delta R_s \, dt \tag{41}$$

Eqn. (41) gives the measure of the errors in stator flux linkage due to the change in stator resistance.

The IOFL controller can be made more reliable if the stator resistance is estimated online during operation of machine. In this paper, an estimator is designed to predict the stator resistance. A signal proportional to the stator resistance change is developed using the error between the reference and actual flux linkage. The estimator observes the actual stator flux (λ_{sa}) and if an ($\Delta\lambda_s$) error between the reference and actual flux linkage is detected, a corresponding change in the stator resistance is made. The estimator is based on the PI controller as shown in Fig. 5. The error in the stator flux is used as an input to the PI estimator. The technique is based on the principle that the change in stator resistance will cause a change in stator current and stator flux linkage λ_{sa}. The error between the actual stator flux (λ_{sa}) and the reference flux is

Fig. 5 : PI Resistance Estimator of SynRM Drive System

proportional to the stator resistance change. The PI resistance estimator of Fig. 5 is described by

$$\Delta R_s = \left(K_P + \frac{K_I}{s} \right) \Delta\lambda_s \tag{42}$$

Where s is Laplace operator and K_P and K_I are the proportional and integral gains of the PI estimator.

The error between the stator flux λ_s and its reference λ_s^* is passed through a low pass filter with a very low cutoff frequency in order to attenuate high frequency component contained in the estimated stator flux. Then the signal is passed through a PI estimator. The output of the PI estimator is the required change of resistance ΔR_s due to change in temperature or frequency. The change of stator resistance ΔR_s is continuously added to the previously estimated stator resistance $R_{s(k-1)}$. This updated stator resistance can be used directly in the controller. One may note that for a given torque reference T_e^*, if y_2^* is set to zero at each Δt step of time, then the reference currents responsible for torque generation, i_{dT}^* and i_{qT}^*, are obtained and λ_s^* can be calculated as

$$\lambda_s^* = \sqrt{L_d^2 i_{dT}^{e*^2} + L_q^2 i_{qT}^{e*^2}} \tag{43}$$

Simulation results

Overall block diagram of the drive system control was shown in Fig.4. Based on IOFL the motor supply voltage is synthesized from stator d and q axis voltage commands (v_d^*, v_q^*), using a two

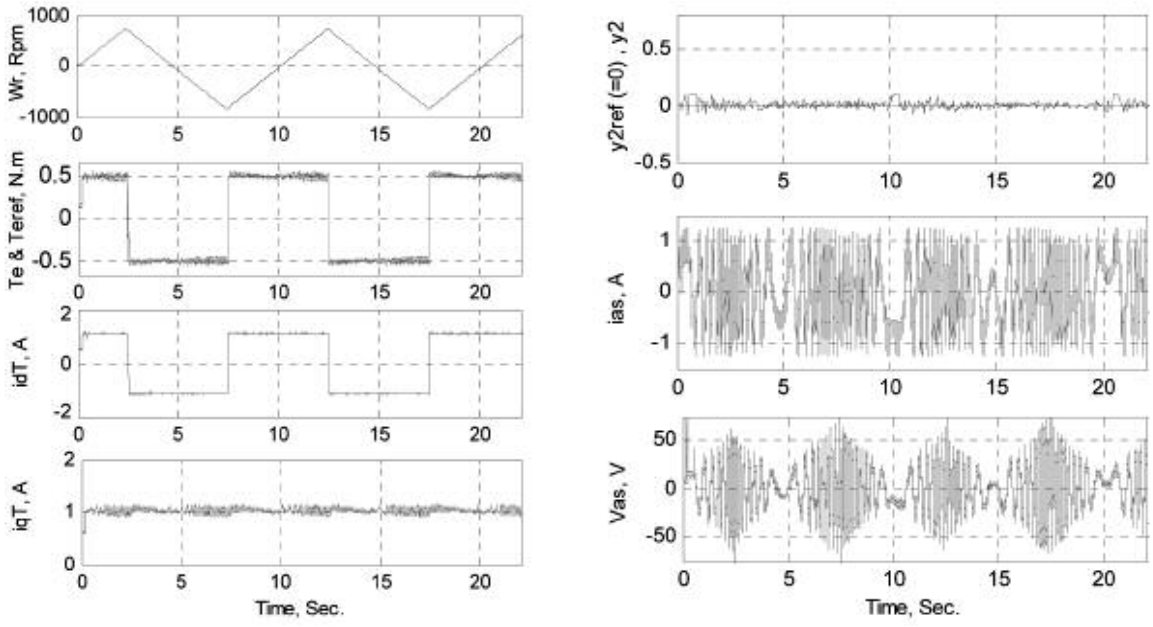

Fig. 6: MTPA Control Strategy Simulation Results

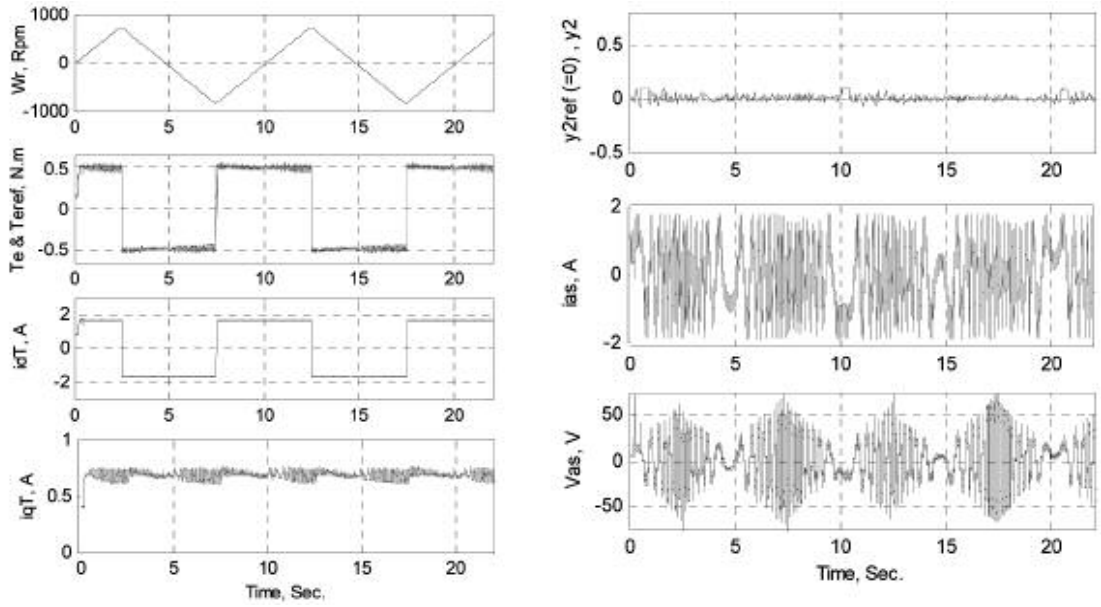

Fig. 7: Efficiency-Optimized Control Strategy Simulation Results

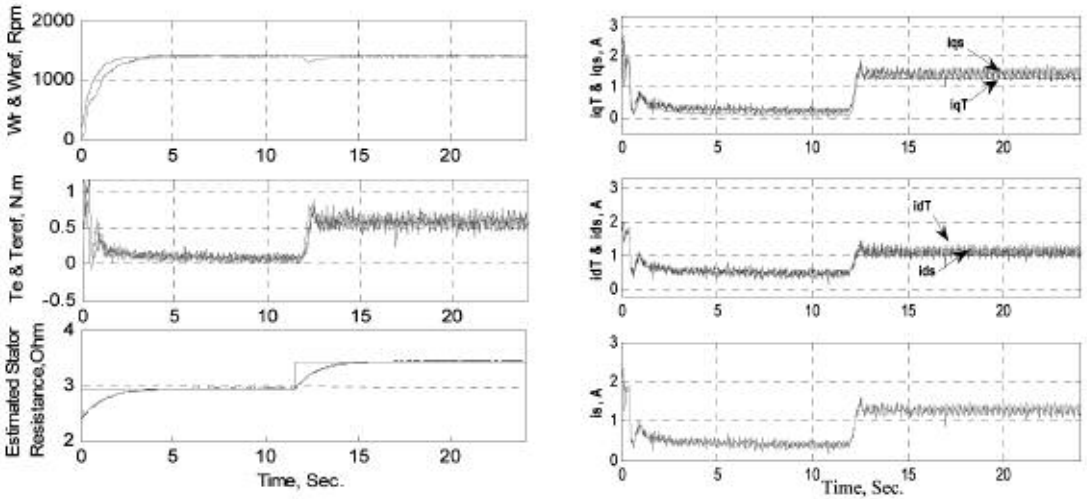

Fig. 8: MTPA Control Strategy Simulation Results (Speed Tracking Control)

level space vector modulation SVM-based PWM inverter. A *C*++ step by step computer program was developed to model the drive system control of Fig.4. In this program, the system dynamic equations are solved by a static Range-Kutta fourth order method. In our proposed control approach the system controller gains are obtained by trial and error method which are given by $K_p = 0.3$, $K_I = 0.05$ and $K_1 = K_2 = 225$. The specifications and parameters of three-phase SynRM used in our simulation program are given in Appendix I. Considering MTPA and Efficiency-Optimized control strategies relating to SynRM, the simulated results are presented in Figs. 6-7. As shown in figures, the proposed controller satisfies both of the control objectives; the torque y_1 and MTPA criteria or Efficiency-Optimized criteria y_2 are well regulated to the respective commands and the internal states (i_d^T, i_q^T) move to the optimal point along the demanded torque curve. The speed ω_m increases and decreases rather linearly which means that the produced torque is regulated well to its desired value by the help of the proposed nonlinear controller. Assuming an exponential speed reference, the simulation results are obtained for MTPA strategy in Fig. 8. From these results a perfect tracking control can be recognized for the two axis currents as well as estimation error in parameter Rs also converges to zero. In addition, torque current and terminal current waveforms have been shown in this figure. The shunt iron loss resistance of the SynRM is responsible for this miss matching.

In order to confirm the improvement of SynRM efficiency through the proposed control algorithm, the efficiency of the SynRM was measured in each case of the conventional controller with constant d-axis current and the proposed controller. At various speed conditions the comparison results of each controller are illustrated in Fig. 9. The overall enhancement in efficiency is seen and is remarkable at lighter load and lower speed conditions.

Experimental setup and results

Exprimental System Setup

For practical evaluation of the actual system performance, a PC-based prototype system was built and tested. The experimental setup corresponding to overall system block diagram shown in Fig. 4 is depicted in Figs. (10-11) and consists of the following sections:

A 0.37 kW three-phase SynRM and a 1.1 kW DC generator as its load; Three-phase voltage source inverter and its isolation board;

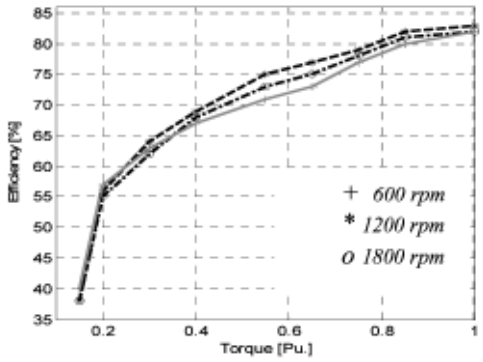

a) constant i_d control

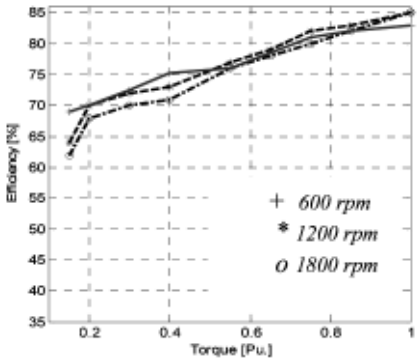

b) Proposed method

c) Efficiency Improvement

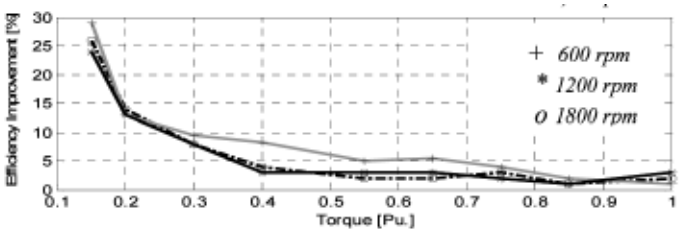

Fig. 9: Efficiency improvement at various Torques and speeds: a) constant i_d control, b) Proposed method, c) Efficiency Improvement

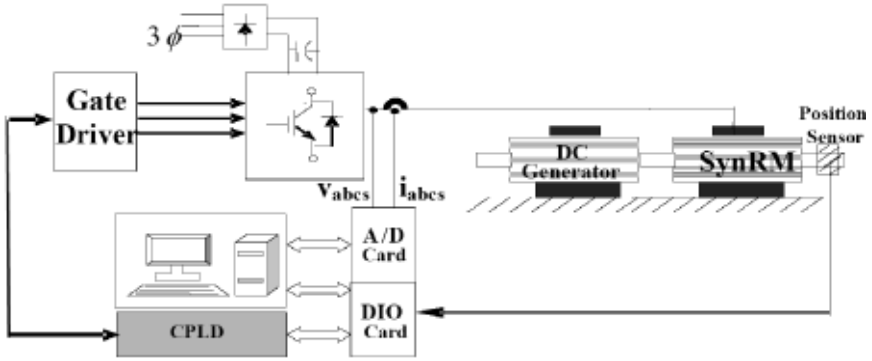

Fig. 10: Laboratory Implementation Block Diagram

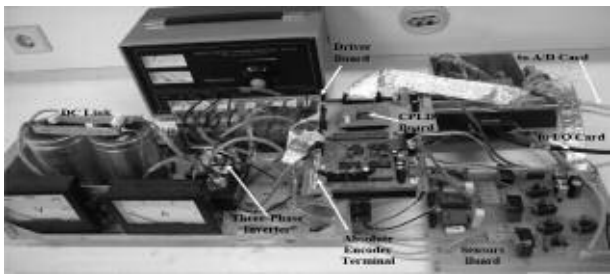

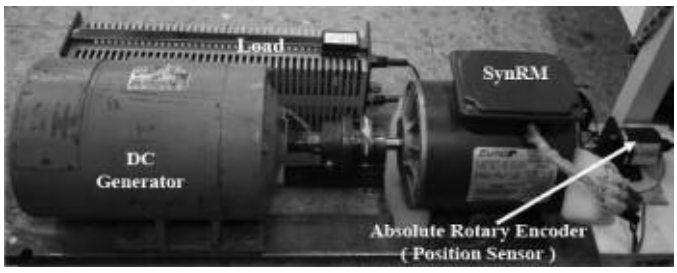

Fig. 11: Experimental Setup

Voltage and current sensors board; 96 bit Advantech digital Input-Output card; 32-channel Advantech A/D converter card; CPLD board and a personal computer (PC) for calculating required signals and viewing the registered waveforms. The 0.37 kW SynRM parameters are reported in Appendix I.

The SynRM is supplied by a three-phase inverter with a symmetrical two level space vector modulation. A Xilinx XC95288xl CPLD has been selected for real time implementation of switching patterns using a switching frequency of 5 kHz.

The CPLD board communicates with PC via the digital Advantech PCI-1753 I/O board. CPLD in experimental setup realizes the following tasks: Switching pattern generation of IGBT switches based on SVM technique, providing a useful dead time in the so-called switching patterns of power switches, generation of the synchronizing signal for data transmission between PC and hardware and shutting down the inverter in the case of emergency conditions such as over current or PC hanging states. The inverter has been designed & implemented specifically for this experiment using SKM75 GD 124 D SEMIKRON module.

The required drive board has been designed by HCPL 316J which is fast and intelligent IGBT driver and guarantees a reliable isolation between the high voltage and control boards. The DC link voltage and stator phase currents and voltages are measured by

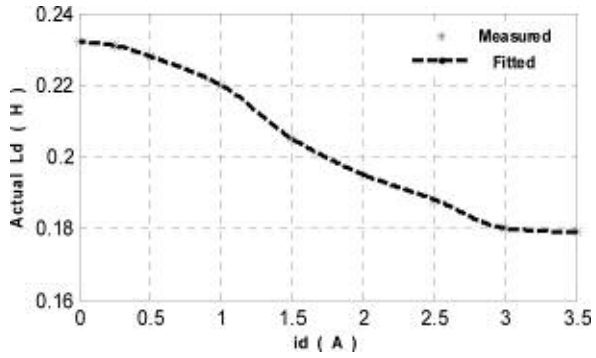

Fig. 12: Variation of L_d with d-axis current i_d

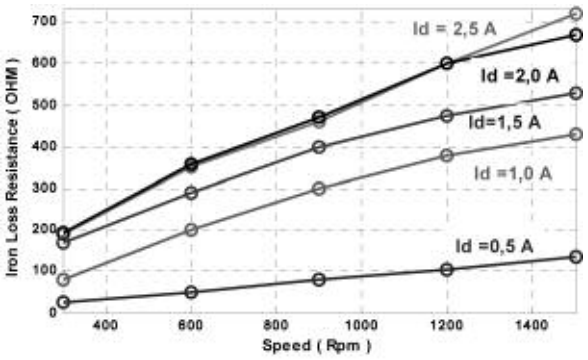

Fig. 13: Measured Iron Loss Resistance R_i

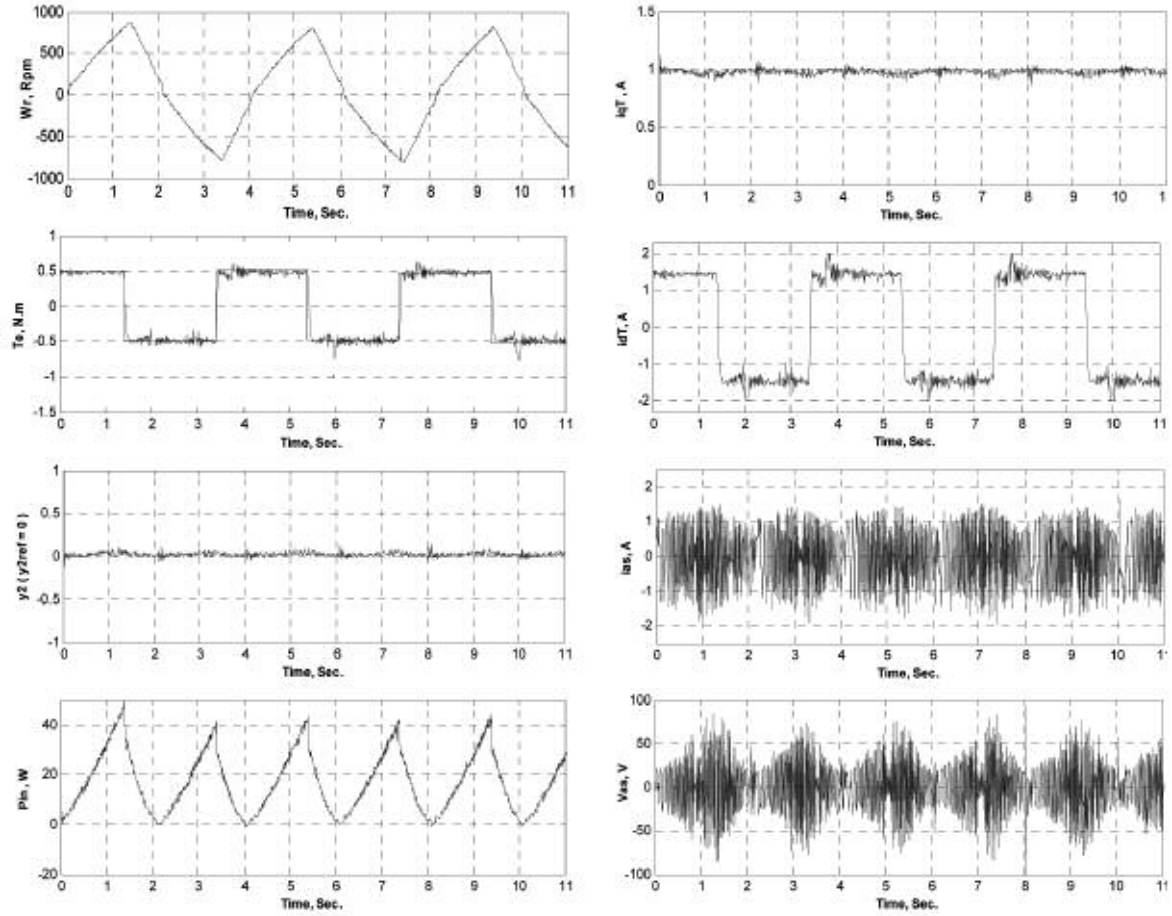

Fig. 14: MTPA Control Strategy Experimental Results

Hall-type LEM sensors. All measured electrical signals are filtered using the separate analogue second order low pass filters and then converted to digital signals using an A/D card with conversion time. The rotor position is measured in respect to axis of stator "A" phase using an AUTONICS absolute encoder with 1024 pulses per round. The output pulse of position sensor is sent to the PC via I/O card.

Experimental results

Using the same conditions adopted to get SynRM simulation results as described in previous section, the experimental results were obtained as shown in Figs. 14-16. The motor d axis inductance L_d versus i_d can be obtained from a practical test, as shown in Fig. 12. The iron loss resistance R_i can be acquired by measuring the input power under no-load condition, and the measured results are plotted in Fig. 13. Since varies with operating frequency and magnetizing current, this value is updated to the controller in real time according to the load condition and speed. For a given load torque, one can see from Figs. 14 and 15 that SynRM input power in Efficiency-Optimized scheme is less than MTPA strategy while stator current amplitude in MTPA strategy is smaller than Efficiency-Optimized scheme. The value of stator resistance R_s is also determined by PI estimator as shown in Fig. 16. In Fig. 17, experimental phase voltage and current waveforms have been shown. A close agreement can be seen between simulation and practical results with little disagreement seen between these two set of results may be because of inaccuracies that exist in our data acquisition system, SVPWM voltage source inverter effects and the dead times of inverter switching signals.

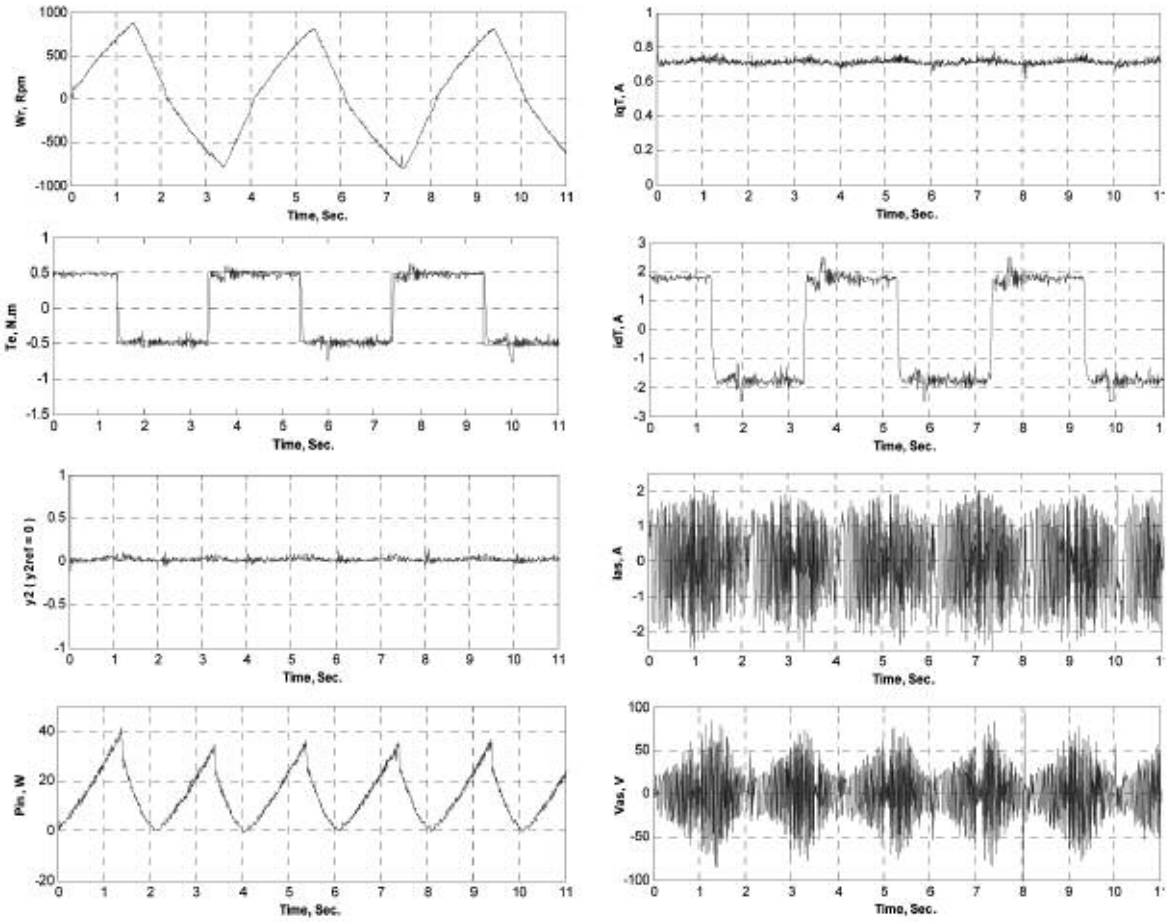

Fig. 15: Efficiency-Optimized Control Strategy Experimental Results

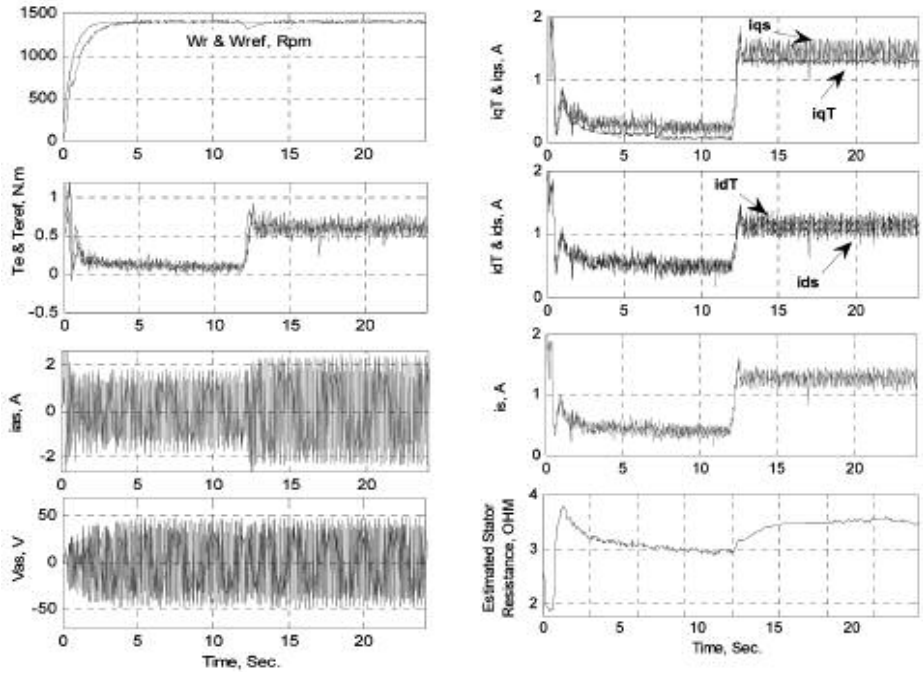

Fig. 16: MTPA Control Strategy

Conclusions

For high dynamic torque regulation and implementation of desirable control strategy (MTPA, efficiency-optimized or minimum input KVA Control) of the SynRM, a nonlinear controller using input–output feedback linearization technique was proposed. The coupling effects and the nonlinearity in the state equation of the SynRM that deteriorate the linear torque–speed characteristics

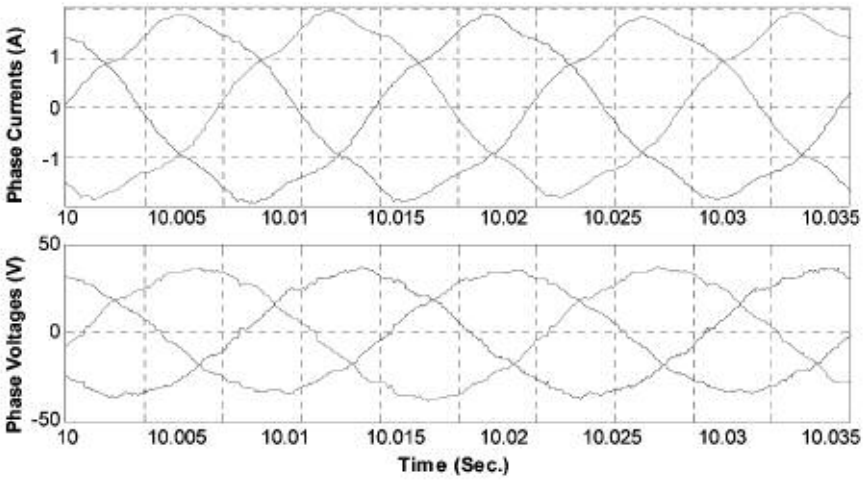

Fig. 17: SynRM Phase Voltage and Current waveforms

were discussed, and it can be concluded that the shunt iron loss resistance of the SynRM is responsible for these aspects. In addition, based on Lagrange's Theorem, some strategy criteria of the SynRM were obtained. The proposed controller directly regulates both the electromagnetic torque and the chosen criterion by selecting these as output variables. The values of stator direct-axis inductance L_d and iron-loss resistance R_i were found from lookup tables and a PI estimator established the value of stator resistance variations. The usefulness of the proposed control scheme was verified by computer simulations and hardware experiments. Close agreement is observed between the results of simulation and experiment, any discrepancy between them is attributed to limitations of the data acquisition system, SV-PWM voltage source inverter effects and the dead times of inverter switching signals.

Appendix I

Table I: Motor Nominal Characteristics		
P_n = 370 W	V_n = 230 V	I_n = 2.8 A
$L_{md,un\ Sat}$ = 232 mH	$I_{ms,\ Sat}$ = 178 mH	L_{mq} = 118 mH
R_{sn} = 2.95 W	f_n = 60 Hz	No. of Poles: 4
T_{en} = 1.9 N.m	J_m = .015 Kg.m^2	B_m = .003 Nm/rad/sec

Appendix II

MTPA Strategy

$$L_f y_1 = \frac{-K_T}{L_d}\{R_s x_1 - L_q(1+\frac{R_s}{R_i})x_2 x_3\}x_2 \frac{-K_T}{L_q}\{R_s x_2 + L_d(1+\frac{R_s}{R_i})x_1 x_3\}x_1 \tag{A1}$$

$$L_f y_2 = \frac{4K_T}{L_d}\{1+\frac{L_d^2}{R_i^2}x_3^2\}\{R_s x_1 - L_q(1+\frac{R_s}{R_i})x_2 x_3\}x_1 - \frac{4K_T}{L_d}\{1+\frac{L_q^2}{R_i^2}x_3^2\}\{R_s x_2 + L_d(1+\frac{R_s}{R_i})x_1 x_3\}x_2 - \frac{4K_T^2}{J_m R_i^2}(L_d^2 x_1^2 - L_q^2 x_2^2)x_1 x_2 x_3 \tag{A2}$$

$$E(X) = \begin{bmatrix} \frac{K_T x_2}{L_d} & \frac{K_T x_1}{L_q} \\ -\frac{4K_T}{L_d}\{1+\frac{L_d^2}{R_i^2}x_3^2\}x_1 & \frac{4K_T}{L_q}\{1+\frac{L_q^2}{R_i^2}x_3^2\}x_2 \end{bmatrix} \tag{A3}$$

Effieciency-optimized Control strategy

$$L_f y_1 = \frac{-K_T}{L_d}\{R_s x_1 - L_q(1+\frac{R_s}{R_i})x_2 x_3\}x_2 \frac{-K_T}{L_q}\{R_s x_2 + L_d(1+\frac{R_s}{R_i})x_1 x_3\}x_1 \tag{A4}$$

$$\begin{aligned} L_f y_2 = {} & \frac{6K_T}{L_d R_i^3}\{R_s + \frac{(R_s+R_i)}{R_i^2}L_d^2 x_3^2\}\{R_s x_1 - L_q(1+\frac{R_s}{R_i})x_2 x_3\}x_1 - \frac{6K_T}{L_q R_i^3}\{R_s + \frac{(R_s+R_i)}{R_i^2}L_q^2 x_3^2\}\{R_s x_2 + L_d(1+\frac{R_s}{R_i})x_1 x_3\}x_2 \\ & - \frac{6K_T^2}{J_m R_i}(1+\frac{R_s}{R_i})(L_d^2 x_1^2 - L_q^2 x_2^2)x_1 x_2 x_3 \end{aligned} \tag{A5}$$

$$E(X)=\begin{bmatrix} \dfrac{K_T x_2}{L_d} & \dfrac{K_T x_1}{L_q} \\ -\dfrac{6K_T}{L_d}\{R_s+\dfrac{(R_s+R_i)}{R_i^2}L_d^2 x_3^2\}x_1 & \dfrac{6K_T}{L_q}\{R_s+\dfrac{(R_s+R_i)}{R_i^2}L_q^2 x_3^2\}x_2 \end{bmatrix} \tag{A6}$$

Min. Input KVA

$$L_f y_1=\frac{-K_T}{L_d}\{-\frac{R_s}{L_d}x_1+\frac{L_q}{L_d}(1+\frac{R_s}{R_i})x_2x_3\}x_2\ \frac{-K_T}{L_q}\{R_s x_2+L_d(1+\frac{R_s}{R_i})x_1x_3\}x_1 \tag{A7}$$

$$L_f y_2=\left\{\frac{-4L_d^3}{R_i^2}x_1^3x_3^2+\frac{x_3}{R_i}\left(L_d-L_q\right)\left(\frac{4x_1^3}{L_d}L_q^2x_2^3-3x_1^2L_d x_2^4\right)\right\}\{-R_s x_1+L_q(1+\frac{R_s}{R_i})x_2x_3\}\left\{\frac{4L_q^3}{R_i^2}x_2^3x_3^2-\frac{x_3}{R_i}\left(L_d-L_q\right)\left(\frac{4x_2^3}{L_q}L_d^2x_1^3-3x_2^2L_q x_1^4\right)\right\}$$
$$\{-R_s x_2-L_d(1+\frac{R_s}{R_i})x_1x_3\}+\left\{\frac{2x_3}{R_i}\left(L_q^4x_2^2-L_d^4x_1^4\right)+\frac{1}{R_i}\left(L_d-L_q\right)\left(L_q^2x_2^3x_1^4-L_d^2x_1^3x_2^4\right)\right\}\frac{P}{2}(\frac{K_T}{J_m}x_1x_2-\frac{T_l}{J_m}) \tag{A8}$$

$$E(X)=\begin{bmatrix} \dfrac{K_T x_2}{L_d} & \dfrac{K_T x_1}{L_q} \\ \left(\dfrac{-4x_3^2}{R_i^2}L_d^4x_1^3-4L_d^2x_1^3-\dfrac{x_3}{R_i}\left(L_d-L_q\right)\left(3L_d^2x_1^2x_2-L_q^2x_2^3\right)\right)\dfrac{1}{L_d} & \left(\dfrac{-4x_3^2}{R_i^2}L_q^4x_1^3+4L_q^2x_2^3+\dfrac{x_3}{R_i}\left(L_d-L_q\right)\left(3L_q^2x_2^2x_1-L_d^2x_1^3\right)\right)\dfrac{1}{L_q} \end{bmatrix} \tag{A9}$$

References

[1]. T. A. Lipo: Synchronous Reluctance Machines-A Viable Alternative for AC Drives?, Electric Machines and Power Systems, vol. 19, pp 659-671, 1991

[2] A. Consoli, F. Russo, G. Scarcella and A. Testa: Low and Zero-Speed sensorless Cotrol of Synchronous Reluctance Motors, IEEE Trans. On Industry Applications, vol. 35, No. 5, pp 1050-1057, 1999

[3]. I. Boldea, N. Muntean and S. A. Nasser: Robust Low Cost Implementation of Vector Control of Reluctance Synchronous Machines, IEEE Proc. Elect. Power Appl., Vol. 141, Issue I, pp 1-6, Jun. 1994

[4] A. Chiba and T. Fukao: A Closed-Loop Operation of Super High-Speed Reluctance Motor for Quick Torque Response, IEEE Trans. on Industry Applications, vol. 28, No. 3, pp 600-606, 1992

[5] T. Senjyu, K. Kinjo, N. Urasaki and K. Uezato: High Efficiency Control of Synchronous Reluctance Motors using Kalman Filter, IEEE Trans. on Industrial Electronics, vol. 50, No. 4, pp 726-732, 2003

[6] R. E. Betz, R. Lagerquist, M. Jovanovic, T. J. E Miller and R. H. Middleton: Control of Synchronous Reluctance Machines, IEEE Trans. on Industry Applications, vol. 29, No. 6, pp 1110-1122, 1993

[7] L. Xu, X. Xu, T. A. Lipo and D. W. Novotry: Vector Control of a Synchronous Reluctance Motor Including Saturation and Iron Loss, IEEE Trans. on Industry Applications, vol. 27, No. 5, pp 977-985, 1991

[8] L. Xu and J. Yao: A Compensated Vector Control of a Synchronous Reluctance Motor Including Saturation and Iron Losses, IEEE Trans. on Industry Applications, vol. 28, No. 6, pp 1330-1338, 1992

[9] T. Lubin, H. Razik and A Rezzoug: Magnetic Saturation Effects on the Control of a Synchronous Reluctance Machine, IEEE Trans. On Energy Conversion, vol. 17, No. 3, pp 356-362, 2002

[10] S. Ichikawa, M. Tomita, S. Doki and S. Okuma: Sensorless Control of Synchronous Reluctance Motors Bassed on Extended EMF Models Considering Magnetic Saturation with Online Parameter Identification, IEEE Trans. On Industry Appl., Vol. 42, No. 5, pp. 1264-1274, Sept./Oct. 2006

[11] E. M. Rashad, T. S. Radwan and M. A. Rahman: A Maximum Torque Vector Control Strategy for Synchronous Reluctance Motors Considering Saturation and Iron Losses, IEEE IAS, pp. 2411-2417, 2004

[12] M.T. Lin, and T.H. Liu: Sensorless synchronous reluctance drive with standstill starting, IEEE Trans. Aero. Electron. Syst., 36, (4), pp. 1232–1241, 2000

[13] T.S. Eldin, W. Dunnigan, J.E. Fletcher, and B.W. Williams: Nonlinear robust control of a vector-controlled synchronous reluctance machine, IEEE Trans. Power Electron., 1999, 14, (6), pp. 1111–1121

[14] S.J .Kang, and S.K. Sul: Highly dynamic torque control of synchronous reluctance motor, IEEE Trans. Power Electron., 13, (4), pp. 793–798, 1998

[15] A. Consoli, C. Cavallars, G. Scarcella,, and A. Testa: Sensorless torque control of synchronous motor drives, IEEE Trans. Power Electron., 15, (1), pp. 28–35, 2000

[16]. T.-H. Liu and H.-H. Hsu: Adaptive controller design for a synchronous reluctance motor drive system with direct torque control, IET Electr. Power Appl., Vol.1, No.5, pp. 815–824 815, 2007

[17]. H. D. Lee, S. J. Kang and S. K. Sul: Efficiency-Optimized Direct Torque Control of Synchronous Reluctance Motor Using Feedback Linearization, IEEE Trans. on Ind. Elec., vol. 46, No. 1, pp 192-198, 1999

[18]. Habetler, T. G., Profumo, F., Griva, G., Pastorelli, M. and Bettini, A.: Stator Resistance Tuning in a Stator Flux Oriented Drive using an Instantaneous Hybrid Flux Estimator, Conf. Record EPE, U.K., vol. 4, 1993, pp. 292-299

[19]. Kerkman, R. J., Seibal, B. J., Rowan, T. M and Schlegel D.: A New Flux and Stator Resistance Identifier for AC Drive Systems, Conf. Record, IEEE-IAS, Florida, Oct. 1995, pp. 310-318

[20]. Mir, S., Elbuluk, M.E and Zinger, D.S: PI and Fuzzy Estimators for Tuning the Stator Resistance in Indirect Torque Control of Induction Machines, IEEE Tran. On Power Electronics, vol. 13, No. 2, March 1998, pp. 279-287

[21]. Tang, L and Rahman, M. F: Investigation of an Improved Flux Estimator of a Direct Torque Controlled Interior Permanent Magnet Synchronous Machine Drive, 35th Annual IEEE Power Electronics Specialists Conf., Aachen, Germany, 2004, pp. 451-457

[22]. Marino, R. and Tomei, P.: Nonlinear Control Design, Prentice Hall, Inc, 1995

The authors

Hossein Abootorabi Zarchi graduated from Isfahan University of Technology, Isfahan/Iran and obtained Master degree from the same University. He is currently a Ph.D student in Isfahan University of Technology and his interest research topics are nonlinear control, fault diagnosis in electromechanical systems, power electronics and variable-speed ac drives.
Email: abootorabi9@yahoo.com

Gholam Reza Arab Markadeh graduated from Isfahan University of Technology, Isfahan/Iran and obtained Master's and Ph.D degrees from the same University. His main area of research is nonlinear control, power electronics and variable-speed ac drives. He is currently an assistant professor at Engineering Department, Shahrekord University, Shahrekord, Iran.
Email: arab-gh@eng.sku.ac.ir

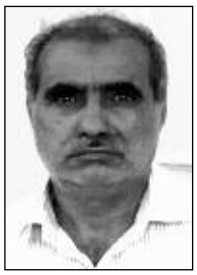

Jafar Soltani graduated from Tabriz University, Tabriz/Iran. He resived Ms.C and Ph.D degrees from UMIST. He is an emeritus professor at Isfahan University of Technology, Isfahan/Iran. His main area of research is electrical machines and drives. He is a member of IEEE and IET. He has published many international journal and conference papers. He also holds a UK patent.
Email: j1234sm@cc.iut.ac.ir

1	Abbreviated Journal Title	ISSN	2008 Total Cites	Impact Factor	5-Year Impact Factor	Immediacy Index	2008 Articles	Cited Half-life	EigenfactorTM Score	Article InfluenceTM Score
2	AAPG BULL	0149-1423	4588	1.364	1.63	0.353	68	>10.0	0.00685	0.8
3	AAPS PHARMSCITECH	1530-9932	1078	1.445		0.09	167	4	0.00355	
4	AATCC REV	1532-8813	252	0.352	0.465	0.091	44	5	0.00141	0.178
534	EPE J	0939-8368	106	0.435		0.2	20	4.9	0.00031	
535	EPIDEMIOL INFECT	0950-2688	4393	2.36	2.337	0.482	199	7	0.01341	0.803
536	EPIDEMIOL PSICHIAT S	189X	323	2.18		2.382	34	2.5	0.00073	

باسمه تعالی

تاریخ:۱۴۰۱/۳/۲۳

فرم خود ارزیابی مقاله ژورنالی

(توسط متقاضی)

همکار ارجمند

با توجه به اهمیت داوری صحیح مقاله ها، خواهشمند است به پرسش های زیر با دقت پاسخ دهید. همچنین، گزارش طرح های پژوهشی، پایان نامه کارشناسی ارشد و رساله دکتری خود را به ضمیمه مدارک تسلیم دارید. درخواست می شود لطفا به همپوشانی آثار، توجه ویژه ای مبذول فرمایید.

شماره ردیف: 4 **عنوان مقاله:**

Direct Torque Control of Synchronous Reluctance Motor using Feedback Linearization Including Saturation and Iron Loss

۱- آیا مقاله ای با محتوای مشابه در جای دیگری چاپ شده است؟ خیر ■ آری☐ نمی دانم☐

۲- آیا این مقاله با مقاله های دیگر شما همپوشانی دارد؟ (*به مانند: روش حل، نتایج و ...*) خیر ☐ آری■ درصد همپوشانی: 30%

شماره ردیف مقاله: 3 عنوان مقاله‌ای که همپوشانی دارد:

Direct torque and flux regulation of synchronous reluctance motor drives based on input–output feedback linearization

۳- درجه علمی مجله علمی پژوهشی معتبر (JCR , Scopus – علمی پژوهشی داخلی) که مقاله در آن منتشر شده است:

عالی☐ بسیار خوب☐ خوب■ متوسط☐ ضعیف☐

٤- محتوای مقاله از نظر ویژگی های زیر چگونه است؟

۱-اعتبار علمی: عالی☐ خوب■ متوسط☐ ضعیف☐

۲- نوآوری و ابتکار: عالی☐ خوب■ متوسط☐ ضعیف☐

۵- آیا مقاله مستخرج از پایان نامه‌ی کارشناسی ارشد و یا از رساله‌ی دکترای جنابعالی می باشد؟

خیر ☐ آری■ درصد همپوشانی:80%

در صورتی که پاسخ به سؤال بالا مثبت باشد، به پرسش های زیر پاسخ فرمایید:

الف- فرض های به کار رفته و محتویات اصلی تا چه حد بر موارد همانند در پایان نامه و یا رساله منطبق است؟

ب- آیا روش تحلیل و یا نتیجه گیری با موارد همانند در پایان نامه و یا رساله مشابهت دارد؟

٦- آیا این مقاله با مقالات کنفرانسی شما همپوشانی دارد؟

خیر■ آری☐ میزان درصد همپوشانی:

شماره ردیف مقاله: عنوان مقاله‌ای که همپوشانی دارد:

۷- آیا این مقاله با طرح های پژوهشی یا طرح اینترنشیپ شما همپوشانی دارد؟ خیر■ آری☐ درصد همپوشانی:

عنوان طرح:

۸- آیا مقاله (برای استادی شما) با مقالات دانشیاری شما همپوشانی دارد ؟ خیر■ آری☐ درصد همپوشانی:

عنوان مقاله‌ای که همپوشانی دارد:

لطفاً چنانچه نظر اصلاحی یا تکمیلی دارید در این صفحه یا در پشت برگه درج فرمایید.

حسین ابوترابی زارچی

امضاء